

Geometry of contact: contact planning for multi-legged robots via spin models duality

Baxi Chong^{*1}, Di Luo^{*2 3 4}, Tianyu Wang^{1 5}, Gabriel B. Margolis⁶, Juntao He^{1 5},
Pulkit Agrawal^{2 6}, Marin Soljačić⁷, and Daniel I. Goldman^{1 5}

¹ Department of Physics, Georgia Institute of Technology, Atlanta, Georgia 30332, USA

²NSF AI Institute for Artificial Intelligence and Fundamental Interactions

³Center for Theoretical Physics, Massachusetts Institute of Technology, Cambridge, MA 02139, USA

⁴Department of Physics, Harvard University, Cambridge, MA 02138, USA

⁵Institute for Robotics and Intelligent Machines, Georgia Institute of Technology, Atlanta, GA, USA

⁶MIT Improbable AI Lab

⁷ Department of Physics, Massachusetts Institute of Technology, Cambridge, MA 02139, USA

Abstract—Contact planning is crucial in locomoting systems. Specifically, appropriate contact planning can enable versatile behaviors (e.g., sidewinding in limbless locomotors) and facilitate speed-dependent gait transitions (e.g., walk-trot-gallop in quadrupedal locomotors). The challenges of contact planning include determining not only the sequence by which contact is made and broken between the locomotor and the environments, but also the sequence of internal shape changes (e.g., body bending and limb shoulder joint oscillation). Most state-of-art contact planning algorithms focused on conventional robots (e.g. biped and quadruped) and conventional tasks (e.g. forward locomotion), and there is a lack of study on general contact planning in multi-legged robots. In this paper, we show that using geometric mechanics framework, we can obtain the global optimal contact sequence given the internal shape changes sequence. Therefore, we simplify the contact planning problem to a graph optimization problem to identify the internal shape changes. Taking advantages of the spatio-temporal symmetry in locomotion, we map the graph optimization problem to special cases of spin models, which allows us to obtain the global optima in polynomial time. We apply our approach to develop new forward and sidewinding behaviors in a hexapod and a 12-legged centipede. We verify our predictions using numerical and robophysical models, and obtain novel and effective locomotion behaviors.

I. INTRODUCTION

Contact planning is crucial for both biological and robotic locomotors. In biological systems, animals with various morphology can coordinate their body segments to make and break contact with substrate. If properly synchronized with internal body movement (e.g., limb retraction/protraction), such sequenced substrate contact can generate effective self-propulsion for stable and deliberate locomotion [18, 19, 23, 15, 22, 32, 2]. However, it can be challenging to replicate biological locomotion in robotic counterparts. For example, uncoordinated contact planning can lead to unstable behaviors in both limbless [7, 32] and legged [35] systems.

In practice, contact planning of legged locomotion has been extensively studied. The template-anchor approach Full and

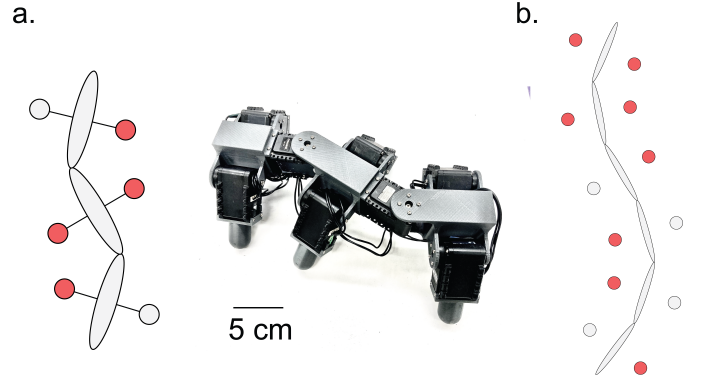


Fig. 1. Multi-legged robot: a geometric and robophysical model (a) (Left) geometric and (right) robophysical hexapod model. (b) Geometric model of a 12-legged centipede.

Koditschek [15] simplifies the control and contact planning. Specifically, in templates¹, the complexity of organisms and terrains is ignored with a simple model to reveal general patterns of dynamics. For example, a template for quadrupedal locomotion includes the gait transition from walk to trot and gallop as speed increases [13, 18, 19]: by prescribing footfall patterns into walk, trot, and gallop, the template simplifies the quadrupedal high-level gait design. When combined with appropriate lower level adaptation to morphological, biomechanical, and environmental details (“anchors” in the parlance of [15]), this approach enables robots with performance approaching those of living systems [4, 20, 39, 2].

Recent work on some bipedal and quadrupedal robot platforms has demonstrated robust and dynamic locomotion. Most recent research on legged robots focused on the anchor design [25, 30, 24, 21, 14], partially because of the well-documented literature on bipedal/quadrupedal templates [42, 15, 18, 19]. Recent anchor designs rely on real-time closed-loop feedback control techniques like model-predictive control [24] or reinforcement learning [21]. While effective, these

¹ Equal contribution. Correspondence to bchong9@gatech.edu, diluo@mit.edu

¹“Template” is a behavior that “contains the smallest number of variables and parameters that exhibits a behavior of interest” [15].

methods demand substantial onboard computation and high-quality proprioceptive or visual sensors.

However, in some applications, sensors can be unreliable and computation scarce. As one example, robots performing search-and-rescue missions must contend with limited vision and possible hardware damage [41]. Similarly, ultra-cheap and/or ultra-small robots require control methods compatible with their limited sensing and compute. To reduce the cost of building robots and generalize the robotic application, researchers have explored robot locomotion frameworks with less dependence on sensors and controls [11]. Specifically, prior work has developed hexapod robots [38], on which the additional legs can help avoid catastrophic failures (e.g., loss of stability). Yet, additional legs require motion pattern coordination and therefore introduce higher dimension for contact planning. To the best of our knowledge, there has been limited research on gait design (contact planning) for hexapod or general multi-legged locomotors.

In this paper, we establish a geometric mechanics model for general multi-legged locomotors. Specifically, in Sec. II, we establish an elaborated physical model of robot-substrate interactions, and describe the contact planning problem for multi-legged locomotors as a graph optimization problem. Further, using the spatio-temporal symmetry properties in locomotion, we map the graph optimization problem to a special case of a spin model [33], which allows us to obtain the global optima in polynomial time. We apply our framework to study hexapod and centipede locomotion. We study the forward and sidewinding behaviors in hexapod locomotion and identify a collection of effective sidewinding gaits for hexapod. We also study centipede (a 12-legged robot) locomotion and obtain effective gaits. We test our hexapod gait predictions using a robophysical model and obtain a good agreement.

II. METHOD

A. Geometric mechanics

1) *Kinematic Reconstruction Equation*: In kinematic systems where inertial effects are negligible (compared with frictional forces), the equations of motion [31] can be approximated as

$$\dot{\xi} = A(\mathbf{r})\dot{\mathbf{r}}, \quad (1)$$

where $\xi = [\xi_x, \xi_y, \xi_\theta]^T$ denotes the body velocity in the forward, lateral, and rotational directions; \mathbf{r} denotes the internal shape variables (joint angles, e.g., $\mathbf{r} = [\alpha_1, \alpha_2]$ in Fig. 2); $A(\mathbf{r})$ is the local connection matrix, which encodes environmental constraints and the conservation of momentum. The local connection matrix A can be numerically derived using resistive force theory (RFT) to model the ground reaction forces (GRF) [26, 40, 43]. Specifically, the net GRF experienced by the locomotor is the sum of the GRF experienced by all segments in stance phase². RFT decomposes the resistive force experienced by a stance-phase segment of a locomotor into

²We consider a segment to be in stance phase if it is in contact with the ground.

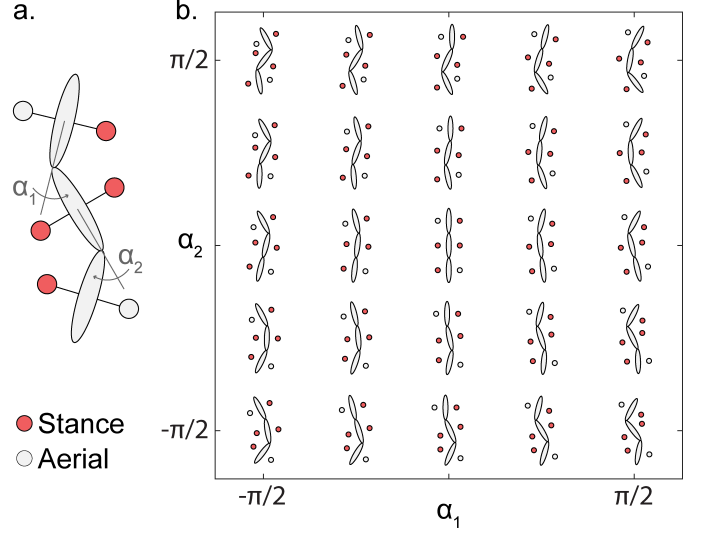


Fig. 2. **Shape space of hexapod** (a) Shape variables and contact patterns. Shape variables (body bending joints) are labeled. Limbs in stance and aerial phases are labeled in red and open circles respectively. (b) Shape space of the geometric hexapod model.

two components: F_{\parallel} and F_{\perp} , reaction force along the direction parallel and perpendicular to the body segment respectively. From geometry and physics of GRF, reaction forces of each segment can be calculated from the body velocity ξ , reduced body shape \mathbf{r} , and reduced shape velocity $\dot{\mathbf{r}}$ [37, 34]. Assuming quasi-static motion, we consider the total net force applied to the system is zero at any instant in time:

$$\mathbf{F} = \sum_{i \in I} [\mathbf{F}_{\parallel}^i(\xi, \mathbf{r}, \dot{\mathbf{r}}) + \mathbf{F}_{\perp}^i(\xi, \mathbf{r}, \dot{\mathbf{r}})] = 0, \quad (2)$$

where I is the collection of all stance-phase segments. At a given body shape \mathbf{r} , Eq.(2) connects the shape velocity $\dot{\mathbf{r}}$ to the body velocity ξ . Therefore, by the implicit function theorem and the linearization process, we can numerically derive the local connection matrix $A(\mathbf{r})$. In our implementation, we compute the solution of Eq.(2) using the MATLAB function *fsolve*. Clearly, the local connection matrix $A(\mathbf{r})$ is dependent on the contact pattern I .

We then consider the relationship between a gait³ and its resulting displacement. The displacement along the gait path ϕ can be obtained by integrating the ordinary differential equation ([17]) below:

$$g(T) = \int_{\phi} L_{g(\mathbf{r})} A(\mathbf{r}) d\mathbf{r}, \quad (3)$$

where $g(\mathbf{r}) = [x(\mathbf{r}), y(\mathbf{r}), \alpha(\mathbf{r})]$ represents the position and rotation of body frame viewed in the world frame at position $\mathbf{r} \in \phi$, T is the time period of a gait cycle, and $g(T) = [\Delta x, \Delta y, \Delta \alpha]$ denotes the translation and rotation of the body frame (w.r.t. the world frame) in one gait cycle. Note that L_g is the rotation matrix with respect to $\alpha(\mathbf{r})$ [34].

The integral of Eq. (3) can be approximated as:

³“Gait” is a closed-loop path in the shape space.

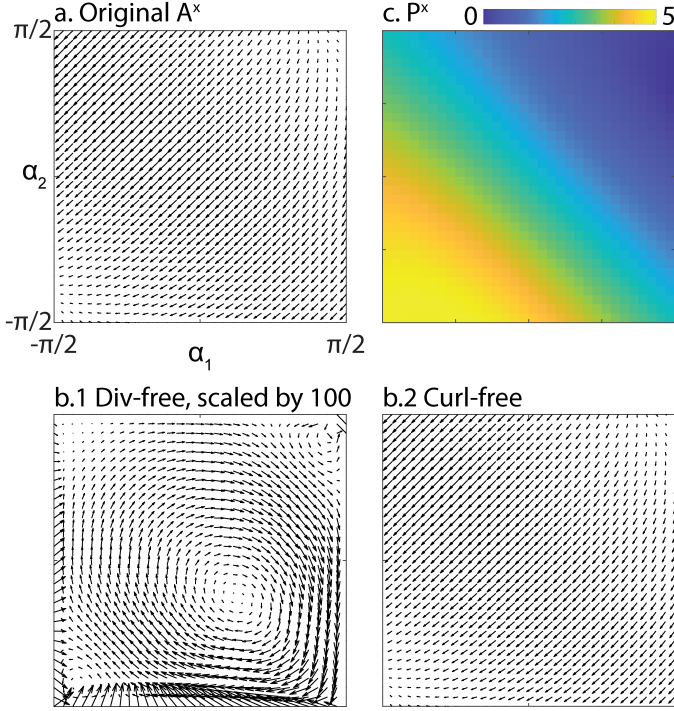


Fig. 3. **Connection vector field and Hodge-Helmholtz decomposition** (a) Connection vector field (A^x) evaluated at contact pattern illustrated in Fig. 2. (b.1) Divergence-free component of the original vector field. Magnitude of the vector field is scaled by 100 for illustration purpose. (b.2) Curl-free component of the original vector field. (c) The potential function computed from the curl-free component of the original vector field. Axes in all panels are identical

$$g(T) \approx \int_{\phi} \mathbf{A}(\mathbf{r}) d\mathbf{r} = \int_{\phi} \begin{bmatrix} A^x(\mathbf{r}) \\ A^y(\mathbf{r}) \\ A^\theta(\mathbf{r}) \end{bmatrix} d\mathbf{r}, \quad (4)$$

where $A^x(\mathbf{r}), A^y(\mathbf{r}), A^\theta(\mathbf{r})$ are the three rows of the local connections respectively denoting forward, lateral, and rotation vector field. The accuracy of the approximation in Eq. 4 can be optimized by properly choosing the body frame [17, 28]. An example of vector field (A^x) is shown in Fig. 3a. With the above derivation, the net displacement over a period can be approximated by the line integral along the gait path over the local connection vector field.

B. Contact sequence optimization

Note in prior section, we only consider the locomotion problem with a fixed contact pattern, i.e., I is independent of shape variables. Now we consider the locomotion problem where the contact pattern changes. First, we will explore the contact planning problem with a known shape change sequence. Specifically, let $Q = \{r_i, i \in \{1, 2, \dots, M\} \mid r_i \in \mathbb{R}^2\}$ be a collection of sequenced shape variables. We define that contact switch can only occur in one of the designated shape variables in Q . Considering a gait path ϕ sequentially connecting all shapes in Q , we aim to identify the optimal

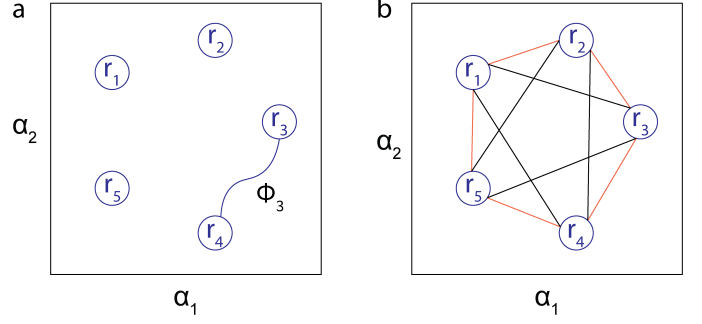


Fig. 4. **Gait paths in the shape space** (a) We sample the shape space with a collection of shape variables $\{r_i\}$. ϕ_3 is an example path connection r_3 to r_4 . ϕ_3 is a fraction of a close-loop gait path connecting all sampled shape variables. (b) An example of a cheating gait path colored in black. We illustrate the unique non-cheating gait path in red color.

contact sequence and gait path ϕ such that the forward (or lateral) displacement is maximized.

We first decompose the closed-loop gait path ϕ into piece-wise curves ϕ_i connecting r_i to r_{i+1} (Fig. 4a). The forward displacement from ϕ is then:

$$\Delta x = \sum_{i=1}^M \int_{\phi_i} A_{I(i)}^x(\mathbf{r}) d\mathbf{r}, \quad (5)$$

where $I(i)$ is the contact pattern along the piece-wise curves ϕ_i , and $A_{I(i)}^x$ is the forward vector field evaluated at the contact pattern $I(i)$. Note that the optimization in Fig. 5 can be decoupled and separately optimized:

$$\max_{\phi, I(\phi)} \Delta x = \max_{\phi, I(\phi)} \sum_{i=1}^M \int_{\phi_i} A_{I(i)}^x(\mathbf{r}) d\mathbf{r} \quad (6)$$

Now we consider the decoupled optimization problem. Using the Hodge-Helmholtz theorem [16], we can decompose a vector field into a curl-free component and a divergence-free component (Fig. 3b). Notably, in most practical locomotion problems on hard ground, the magnitude of divergence-free component is negligible compared with the curl-free component [6, 10, 1], which allows us to focus on the curl-free component of the vector field. For curl-free vector fields, the line-integral is path-independent. Let $P_{I(i)}^x$ be the potential functions of the curl-free components in $A_{I(i)}^x$ (Fig. 3c), we can further simplify Eq. 6 to:

$$\max_{\phi, I(\phi)} \Delta x = \max_{\phi, I(\phi)} \sum_{i=1}^M (P_{I(i)}^x(r_i) - P_{I(i)}^x(r_{i+1})). \quad (7)$$

Thus, with the linear and decoupled form, we simplify the contact planning problem to a linear optimization problem in Eq. 7.

C. Shape change sequence optimization

In the prior section, we assume a pre-fixed shape change sequence and obtain a linear optimization problem formulation

for contact planning problem. We then explore the shape change sequence optimization. First, we sample some shapes in the shape space. Let $Q_{all} = \{r_i, i \in \{1, 2, \dots, M\} \mid r_i \in \mathbb{R}^2\}$ be a collection of sampled shape variables. Let I_{all} (with N elements) be a collection of contact states of a multi-legged locomotor. The displacement optimization on $\Delta x(C)$ can be approximated as:

$$\max_{C, I(C)} \sum_{i \in C} (P_{I(i)}^x(r_{c(i)}) - P_{I(i)}^x(r_{c(i+1)})), \quad (8)$$

where $C \subset M$ is the ordered shape changes, and $\Delta x(C)$ is the resulting displacement. Note that C specifies not only the shapes, but also the sequence of shape changes. In other words, even with the same elements, there could still be different combination of sequences in C . However, many of the combination of sequences can be considered as ‘cheating’. For example, consider a collection of shapes in Fig. 4b with two combination of sequences colored in red and black. In our framework, we seek to maximize the displacement within *one* period. Therefore, the black path in Fig. 4b has an unfair advantage over the red path in Fig. 4b, because the black path winds around the origin twice in one period. To avoid ‘cheating’ and simplify our analysis, we define that the shape can only change in one direction (e.g., clockwise). In this way, given elements in C , there is only one valid path connecting all elements.

In practice, it will always cost finite time and energy to change contact patterns. To count for such cost, we introduce some penalties in contact switching to the cost function.

$$\max_{C, I(C)} \left(-\lambda S(C) + \sum_{i \in C} (P_{I(i)}^x(r_{c(i)}) - P_{I(i)}^x(r_{c(i+1)})) \right), \quad (9)$$

where C is a cycle on the graph, $S(C)$ is the number of contact switch over the path C , and λ is some penalty coefficient. Note that given the explicit physical meaning, we posit that such penalty coefficient λ could be empirically measured in future work. Given the discrete nature of Eq. 9, it can be formulated as a graph optimization problem.

We can further formulate the above optimization problem on as a graph optimization problem. Define V as a collection of nodes v_{ij} , where the index j denotes the shape and the index i denotes the contact pattern. At each time step, we can either change contact pattern or shape. Thus, an edge exists connecting two vertices v_{ij} and v_{kl} if $i = k$ or $j = l$. Let d be a set of weights on edges. For an edge connecting v_{ij} and v_{il} , its weight $d_{ijil} = P_{I(i)}^x(r_j) - P_{I(i)}^x(r_l)$. Note that the weight d_{ijil} can be negative. For an edge connecting v_{ij} and v_{kj} , its weight d_{ijkj} is 0, i.e., changing the contact pattern at a fixed shape will not cause displacement. With the above notation, the optimization problem in Eq. 9 can be reformulated as to find a cycle C , such that the sum of weights along C adding together with $-\lambda S(C)$ is maximal.

Because of the path-independence of connection vector field, we identify the following properties of d_{ijil} : (1) Anti-symmetry: $d_{ijil} = -d_{ilij}$, and (2) Additive: $d_{ijil} + d_{iljk} = d_{ijkj}$.

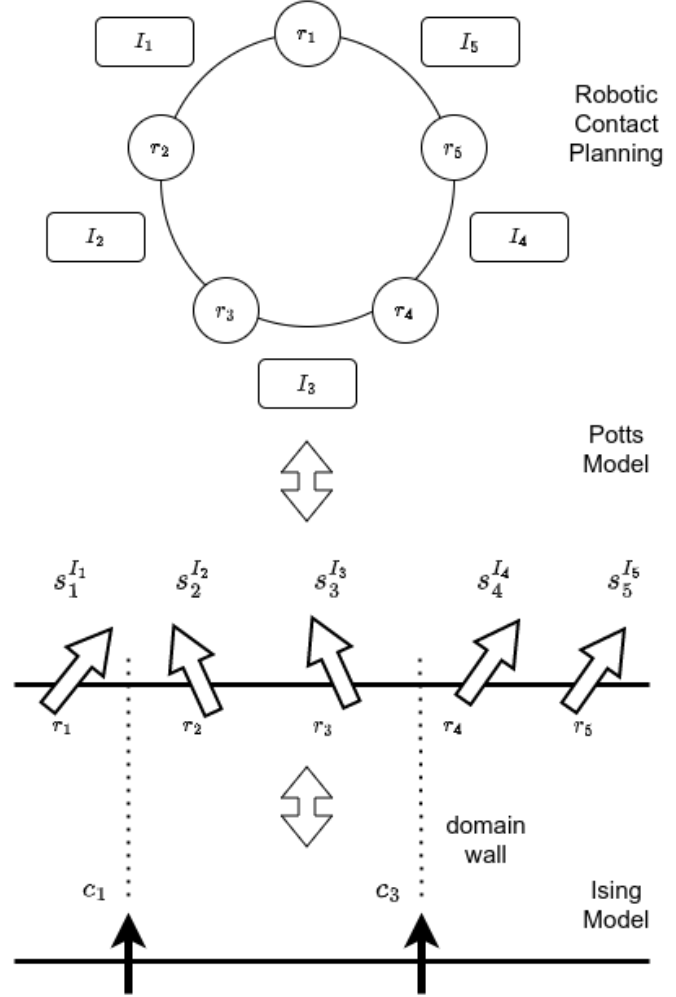


Fig. 5. (Top) Mapping between robotic contact pattern and Potts model. (Bottom) Duality between Potts model and Ising model.

III. SPIN MODELS MAPPINGS AND SOLUTIONS

In general, the coupled contact planning and the shape change optimization problem requires search in a space of size N^M where N is the number of contact patterns and M is the number of shape variables. A brute-force search will scale poorly as the number of legs and joints increases. Instead, to obtain a solution efficiently, we develop a connection between the gait optimization problem and two spin models from physics, the Potts model [36] and the Ising model [33]. In this framework, the optimal shape sequence is equivalent to the ground state of the spin models. In this section, we describe the mappings to the Potts model and the Ising Model and how it exploits the special structure of the problem to enable efficient gait optimization.

We start with mapping the shape sequence problem to a Z_N -spin model. A Z_N -spin model considers an array of M spins sitting on M sites, where each spin has N internal states. Each spin can interact with each other or experience an

onsite magnetic field. This model is well-known to describe magnetism in physics where each spin can be thought of as a small magnet. In particular, for $N = 2$ it reduces to the famous Ising model [33]. It is known that the Ising models have deep connections to graph optimization problems and provide equivalent formulation of many NP-complete and NP-hard problems [29].

A. Potts Model

If we treat the shape variable r_j as the site index j and the contact pattern I_j as the spin internal state, the pair (r_j, I_j) can be mapped to a spin variable s_j^i (or equivalently s_j^I in Fig. 5) at site j . the displacement $P_{I(i)}^x(r_{c(j)}) - P_{I(i)}^x(r_{c(j+1)})$ can be associated with the onsite magnetic field energy $d'_{ij(j+1)} s_j^i$ of the spin variable by defining $s_j^i = e^{2\pi i j/N}$ and $d'_{ij(j+1)} = d_{ij(j+1)} e^{-2\pi i j/N}$. Here d'_{ij} is interpreted as the onsite magnetic field for the Z_N -spin model. Since the shape sequence optimization problem is defined on a loop, it follows that it can be mapped to a Z_N -spin model with periodic boundary condition as follows:

$$H = - \sum_j d'_{ij(j+1)} s_j^i \quad (10)$$

The optimal shape sequence that maximizes Eq. 8 is equivalent to the ground state of the Hamiltonian which minimizes the energy. In this case, the ground state is achieved by each individual spin s_j^i follows the largest $d_{ij(j+1)}$. This is also known as the greedy solution. Translating back to the shape sequence language, we have the greedy algorithm as follows.

Greedy algorithm. The solution of optimal displacement in Eq. 8 is given by

$$\Delta x(C) = \sum_{i \in C} \max_{I(i)} (P_{I(i)}^x(r_{c(i)}) - P_{I(i)}^x(r_{c(i+1)})), \quad (11)$$

For each $r_{c(i)}$ we choose the $I(i)$ that maximizes $P_{I(i)}^x(r_{c(i)}) - P_{I(i)}^x(r_{c(i+1)})$. \square

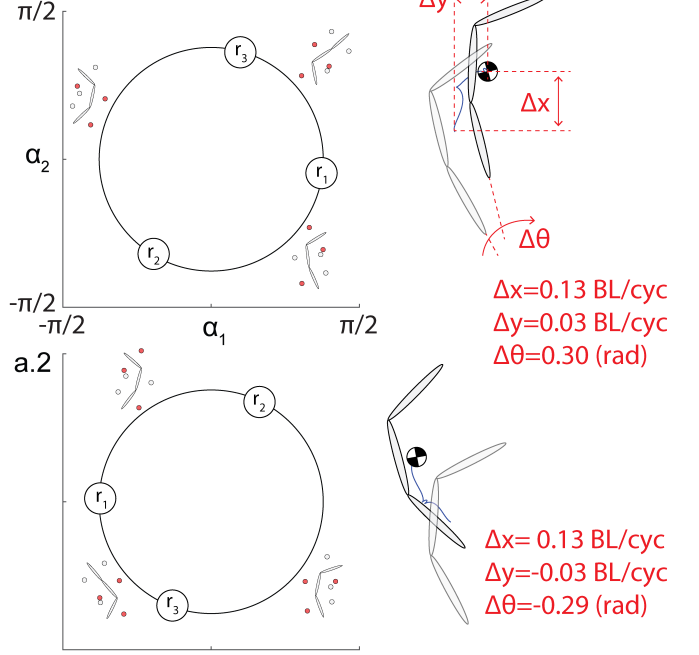
If we further consider the cost of changing contact pattern with penalty λ in Eq. 9, then it is equivalent to introducing a nearest spin interaction with coupling λ , which gives rise to a Potts model [36] with a nonuniform magnetic field

$$H_s = - \sum_j d'_{ij(j+1)} s_j^i - \lambda \delta_{s_j^i, s_{j+1}^i} \quad (12)$$

where $\delta_{s_j^i, s_{j+1}^i} = 1$ if $s_j^i = s_{j+1}^i$ and 0 otherwise.

The mapping between the shape sequence and the Potts model is also described in the upper part of Fig. 5. For this model, the search complexity is N^M . The ground state is expected to have different phenomena depending on λ . For small λ , it is disordered, where each spin follows the local field and the optimal shape sequence is close to the greedy solution. For large λ , the spins align and it is ferromagnetic. The optimal shape sequence gets close to a uniform gait pattern or gait pattern with only a few jumps.

a.1 Contact planning



b. Experiments

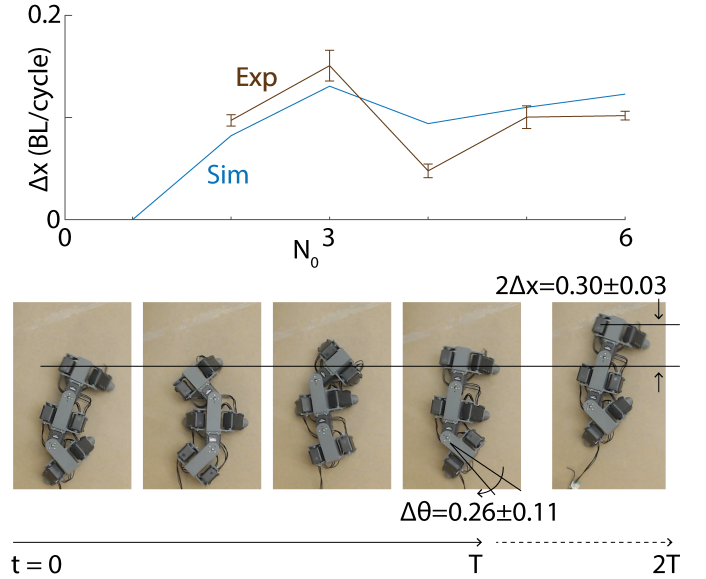
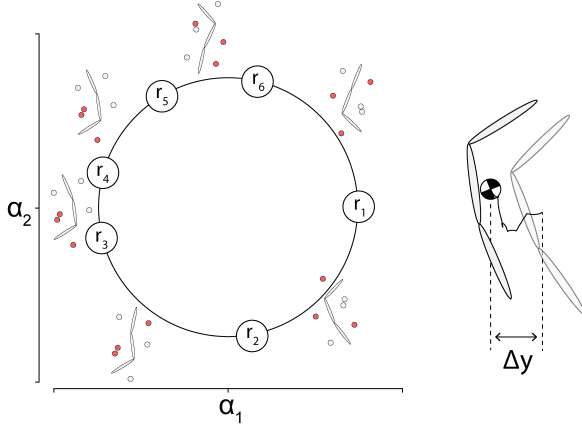


Fig. 6. **Contact planning for hexapod forward locomotion** (a.1) Contact planning for sidewinding hexapod gaits with six contact pattern changes (six-beat) per gait cycle. In the left panel, we illustrate the contact pattern sequence as well as the shape change. In the right panel, we illustrate the net displacement resulting from the contact planning. Axes in all panels are identical. (a.2) Gait formulation and resulting displacements for the anti-symmetric gaits are illustrated. (b) Numerical and experimental verification. (Top) Good agreement between numerical simulation and experiments for sidewinding gaits with different (N_0 , the number of contact pattern changes) (Bottom) Snapshots of robot implementing six-beat gaits ($N_0 = 6$).

B. Ground State Duality to Ising Model

For the Potts model in Eq. 12, we further define a domain wall c_{j+1} to be the existence of a different spin configuration between s_j and s_{j+1} , where $c_{j+1} = 1$ if the domain wall exists

a. Contact planning



b. Experiments

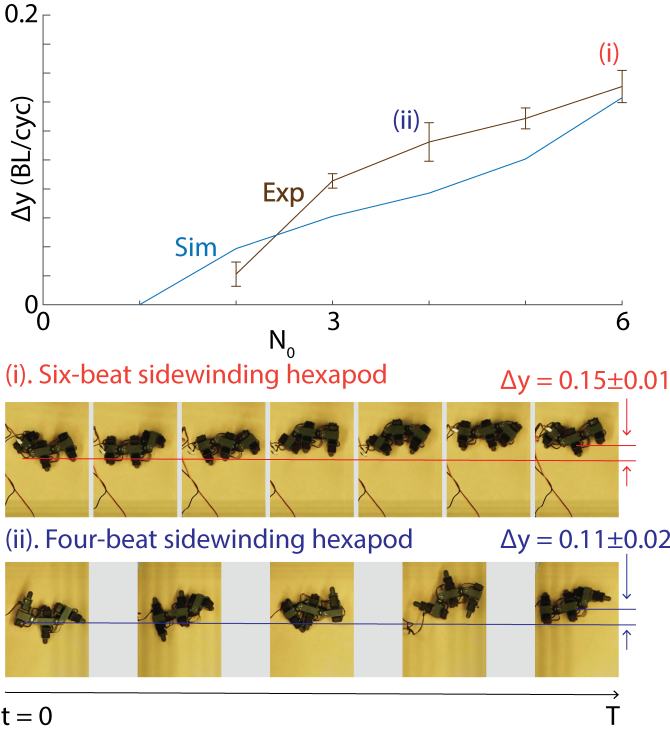


Fig. 7. **Contact planning for sidewinding hexapod** (a) Contact planning for sidewinding hexapod gaits with six contact pattern changes (six-beat) per gait cycle. In the left panel, we illustrate the contact pattern sequence as well as the shape change. In the right panel, we illustrate the net displacement resulting from the contact planning. The axes of shape space is identical to Fig. 6a. (b) Numerical and experimental verification. (Top) Good agreement between numerical simulation and experiments for sidewinding gaits with different (N_0 , the number of contact pattern changes) (Bottom) Snapshots of robot implementing six-beat (i, $N_0 = 6$) and four-beat (ii, $N_0 = 6$) gaits.

and otherwise 0. The mapping between the Potts model and the Ising model is shown in the bottom part of Fig. 5. It follows that we can establish the ground state duality between Potts model and a long-range Ising model using the domain wall mapping and the additive property of d_{ijl} .

Theorem 1. *The Potts model in Eq. 12 with d_{ijl} satisfying the additive property has the same ground state energy as the*

following Ising model with long range couplings J_{jl} .

$$H_c = - \sum_j J_{jl} c_j c_l - \lambda \sum_i c_i \quad (13)$$

where $J_{jl} = \max_i d_{ijl}$.

Proof. Our goal is to show that Eq. 12 and Eq. 13 admit the same ground state energy. To achieve that, it is sufficient to show each term in Eq. 12 can be transformed to a corresponding term in Eq. 13. Consider that there are K locations that the spins do not align with each other in the Potts model, which is equivalent to K domain walls in the Ising model. This costs energy $K\lambda$ from $\lambda s_j^i s_{j+1}^i$ in Eq. 12 and correspondingly from $\lambda \sum_i c_i$ in Eq. 13. For every fixed K , the minimization of Eq. 12 is equivalent to minimize $-\sum_j d'_{ij(j+1)} s_j^i$. This can be achieved by choosing the maximal $\sum_{k=j}^{l-1} d_{ik(k+1)}$ between two domain walls c_j and c_l . Due to the additive property of d_{ijl} , $\sum_{k=j}^{l-1} d_{ik(k+1)} = d_{ijl}$. It results in the term $-\sum_j J_{jl} c_j c_l$ with $J_{jl} = \max_i d_{ijl}$ in Eq. 13. \square

We note that in general Potts model would not be dual to Ising model due to the fact that they have different spin symmetries. However, duality here comes from that we only study the ground state and additive property of d_{ijl} which is special in the robotic contact problem. The mapping reduces the complexity of the original problem from N^M to 2^M . Based on the Ising model Hamiltonian, we develop a domain-wall search algorithm.

Domain-wall search algorithm. Specify the number of domain-walls or jumps K to be searched. Compute the energy $-\sum J_{ij} c_j c_i$ of all M -site spin configurations which have K numbers of $c_j = 1$. Choose the lowest energy configuration among all as the solution and translate it back the shape sequence according to the mapping. \square

There are several advantages of the duality and the domain-wall search algorithm. First, it is independent of the number of shape variables N so that one can always work with a lower degree representation Z_2 -spin instead of a Z_N -spin. This is in particularly helpful for generalization to multi-legged robot with many shape variables. Second, the domain wall has a natural interpretation as the jump in the shape sequence problem. In practice, if we would like to have small number of jumps K , it is equivalent to impose total spin symmetry number or magnetization K to the model. Without such symmetry the original model in Eq. 13 lives in a Hilbert space of size 2^M where M is the number of the shape variables, while the symmetry constraint helps to reduce the Hilbert space complexity to $\text{Cr}(M, K)$. We can also ignore the penalty term λ in this dual formulation within a fixed spin symmetric sector since the penalty will only contribute a constant shift to the energy in the same sector. It is worth notice that for large number of jumps $K \sim M/2$, $\text{Cr}(M, K) \sim 2^M / \sqrt{M}$ has nearly exponential scaling [12], which opens up opportunities for machine learning applications on dimensional reduction and efficient approximation.

IV. EXPERIMENTAL SETUP

To test our method, we employed a hexapod robot featuring two rotational degrees of freedom in the body and one rotational degree of freedom in each leg. The elongated body, measuring 30 cm in length, is segmented by bending joints that allow for rotations of up to ± 90 degrees. Each segment is equipped with limbs on both sides, which can be lifted and landed through control of the rotational joint at the shoulder. All rotational joints are actuated by Dynamixel AX-12A servo motors, and the body linkages and appendages are 3D-printed using PLA material. During experiments, the body is raised up to 5 cm off the ground, and foot tips were set to be lifted up to 2 cm off the ground. The experiments took place on a flat, hard surface and were based on the assumption of dry Coulomb kinetic friction with a foot-ground friction coefficient $\mu = 0.35 \pm 0.06$. Direct joint angle set-point commands were used to control the robot's movements. Each gait was tested through three repeat experiments, with the robot executing five full cycles per experiment.

The motion of the robot motion was monitored in its position space using an OptiTrack motion capture system comprised of 6 Flex 13 cameras. The 3D positions of IR reflective markers, distributed along the robot body, were recorded at a frame rate of 120 FPS. The data was collected as the robot executed five gait cycles, from the start of the first configuration to the end of the last. The displacement was calculated as the projection of the geometry center trajectory onto the forward/horizontal axes.

V. RESULTS

A. Forward hexapod

We first apply our framework to study hexapod forward locomotion. We consider stable contact patterns (for hexapod) as at least three legs are in stance phase. We consider the unilateral support⁴ as unstable contact patterns. Thus, we have 20 contact patterns in total. We sample the shape space by a circular prescription: $\alpha_1 = \pi/3 \sin(\tau)$, $\alpha_2 = \pi/3 \cos(\tau)$, and τ is uniformly sampled over a period.

In robot locomotion, most unstable behaviors in legged locomotion occur during the contact switch [3, 27]. To avoid excessive contact switches, we explore a hexapod forward gait subject to N_0 number of contact pattern changes, and consider the hexapod gaits as a function of N_0 . Applying our framework, we identify five hexapod forward gaits with $N_0 \in [2, \dots 6]$. Examples of $N_0 = 3$ are illustrated in Fig 6a.

We verify our identified gait using numerical simulation [8]. We quantify the displacement in the units of body length travelled per cycle (BL/cyc). We notice that accompanied by the large translation in forward-direction (Δx), there is non-negligible lateral translation (Δy) and net rotation ($\Delta \theta$). The emergence of non-negligible lateral translation and rotation can introduce additional challenge to navigate the robot. Thus, we proceed to minimize Δx and $\Delta \theta$ associated with the forward locomotion.

⁴Three legs in stance phase are on the same (either left or right) side.

We observe that the local connection matrix is symmetric. For any contact pattern $I(i)$, we can obtain its anti-symmetric contact pattern $I'(i)$ such that the contact states of contralateral legs (left and right legs connected to the same body segment) are flipped (Fig. 6.a). From symmetry, we know that: $A_{I(i)}^x(\mathbf{r}) = A_{I'(i)}^x(-\mathbf{r})$, $A_{I(i)}^y(\mathbf{r}) = -A_{I'(i)}^y(-\mathbf{r})$, $A_{I(i)}^\theta(\mathbf{r}) = -A_{I'(i)}^\theta(-\mathbf{r})$. In other words, with both shape symmetry (e.g., \mathbf{r} and $-\mathbf{r}$) and contact symmetry (e.g., $I(i)$ to $I'(i)$), we can preserve the forward velocity (ξ_x) with opposite lateral and rotational velocity (ξ_y and ξ_θ). Thus, we know that for any gait, there exists its anti-symmetric gait with the same forward displacement but opposite lateral displacement and rotation. An example of anti-symmetric gait is shown in the right panel of Fig. 6.a. When we execute a gait and its anti-symmetric gait, we can eliminate the unwanted lateral and rotational displacement and obtain forward-only locomotion.

We test our identified gaits on a robophysical hexapod model. We illustrate that the inclusion of anti-symmetric gaits can eliminate emergence of lateral and rotational displacement. We obtain good agreement between robophysical experiments and numerical simulation (Fig. 6.b). Further, we identify hexapod gaits with forward speed up to 0.15 BL/cyc, which we consider as effective given the relatively short legs (leg length ~ 0.1 BL).

B. Sidewinding hexapod

Multi-legged locomotors are stereotyped to have better capability to locomote forward instead of sideways, partially because of limb protraction/retraction movements are limited in the fore-aft directions (i.e., no direct contribution from limbs to generate sideway locomotion). Recent work [5] on quadrupeds revealed that with proper body bending coordination, sideway behavior is possible but with relatively low speed (< 0.1 BL/cycle). Here, we study the sideway behavior (sidewinding) of hexapod. We posit that with appropriate contact planning, we can enable novel sidewinding behavior of hexapod.

Using the same shape and contact pattern samples from Sec. V-A, we identify sidewinding hexapod gaits as a function of N_0 . An example of $N_0 = 6$ is shown in Fig. 7. We first evaluate the effectiveness of hexapod sidewinding gaits using numerical simulation [8]. We notice that hexapod sidewinding gaits have comparable velocity (0.15 ± 0.01 BL/cyc) as the hexapod forward gaits.

Finally, we test our identified gaits on robophysical model and obtain good agreement with the numerical simulation. We illustrate the snapshots of robot implementing hexapod sidewinding gaits in Fig. 7b.

C. Sidewinding centipede

Centipede locomotion is challenging partially because of the large number of contact states from the many legs [9]. Notably, in our framework, the computational complexity does not scale with the increases in legs. Therefore, we posit that our framework can offer novel insights into centipede locomotion. In this section, we illustrate the generality of our framework by designing sidewinding gaits for a 12-legged centipede

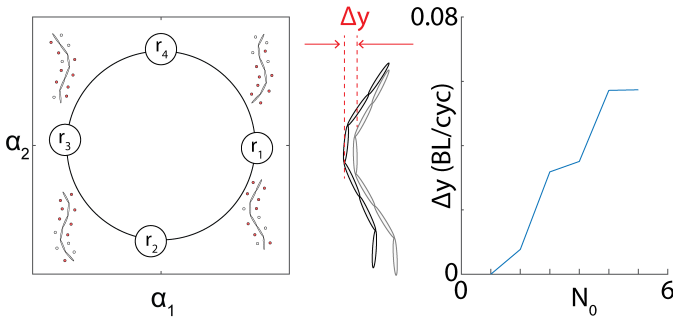


Fig. 8. **Contact planning for sidewinding centipede** (Left) Contact planning for sidewinding centipede gaits with four contact pattern changes (four-beat) per gait cycle. (Mid) The net displacement resulting from the contact planning. (Right) Numerical simulation for sidewinding centipede gaits subject to different N_0 .

locomotor. For simplicity, we consider contact patterns with at least eight legs are in stance phase. Thus, we have 794 contact patterns in total. We sample the shape variable using the shape basis function [9].

Using our framework, we illustrate effective sidewinding gaits in Fig. 8. From numerical simulation, we notice that the centipede sidewinding gaits have comparable absolute lateral displacement. However, since centipedes have much longer body length, the normalized lateral displacement (BL/cyc) is significantly lower in centipede than hexapod ($0.06BL/cyc$). With this observation, we hypothesize that the addition in longitudinal length (increasing the leg number) will not improve the locomotors' capability of the sideways locomotion.

VI. CONCLUSION

In this paper, we built a geometric mechanics model for general multi-legged locomotion and simplify the contact planning problem to a graph optimization problem. We further develop the mapping between the contact planning problem to both the Potts model and the Ising model, which allows us to solve the optimal shape sequence in polynomial time. We use our framework to study hexapod and centipede (12-legged) locomotion. We obtain effective forward and sidewinding gaits for hexapod in both forward and lateral directions. Further, we identify a collection of gaits as a function of N_0 , the number of contact changes. We test our prediction on robophysical models. Our work provides a general approach for studying the locomotion of multi-legged robots and the reformulation of the graph optimization problem and spin models open up future opportunities for applications of machine learning.

In current work, we investigated the locomotion on flat terrains with precise execution of contact patterns. However, in practice, robot locomotion can experience uncertainty in contact patterns. In future work, it is beneficial to establish a probability model on the contact pattern execution related to the finite temperature and entropy properties of the spin models. In doing so, we hypothesize that there exist gaits that are robust over contact uncertainty for reliable locomotion on noisy landscapes. Such robustness then paves ways towards

machines that can traverse complex environments with minimal sensing and feedback controls.

ACKNOWLEDGMENT

The authors are grateful for funding from NSF-Simons Southeast Center for Mathematics and Biology (Simons Foundation SFARI 594594), Army Research Office (ARO) MURI program, Army Research Office Grant W911NF-11-1-0514 and a Dunn Family Professorship, the NSF AI Institute for Artificial Intelligence and Fundamental Interactions (IAIFI).

REFERENCES

- [1] Silas Alben. Efficient sliding locomotion with isotropic friction. *Physical Review E*, 99(6):062402, 2019.
- [2] Henry C Astley, Chaohui Gong, Jin Dai, Matthew Travers, Miguel M Serrano, Patricio A Vela, Howie Choset, Joseph R Mendelson, David L Hu, and Daniel I Goldman. Modulation of orthogonal body waves enables high maneuverability in sidewinding locomotion. *Proceedings of the National Academy of Sciences*, 112(19): 6200–6205, 2015.
- [3] Long Bai, Hao Hu, Xiaohong Chen, Yuanxi Sun, Chaoyang Ma, and Yuanhong Zhong. Cpg-based gait generation of the curved-leg hexapod robot with smooth gait transition. *Sensors*, 19(17):3705, 2019.
- [4] Pranav A Bhounsule, Jason Cortell, and Andy Ruina. Design and control of ranger: an energy-efficient, dynamic walking robot. In *Adaptive Mobile Robotics*, pages 441–448. World Scientific, 2012.
- [5] Baxi Chong, Yasemin Ozkan Aydin, Chaohui Gong, Guillaume Sartoretti, Yunjin Wu, Jennifer M Rieser, Haosen Xing, Perrin E Schiebel, Jeffery W Rankin, Krijn B Michel, et al. Coordination of lateral body bending and leg movements for sprawled posture quadrupedal locomotion. *The International Journal of Robotics Research*, page 0278364921991158, 2021.
- [6] Baxi Chong, Tianyu Wang, Bo Lin, Shengkai Li, Howie Choset, Grigoriy Blekherman, and Daniel I Goldman. Moving sidewinding forward: optimizing contact patterns for limbless robots via geometric mechanics. In *Robotics: Science and Systems*, 2021.
- [7] Baxi Chong, Tianyu Wang, Jennifer M Rieser, Bo Lin, Abdul Kaba, Grigoriy Blekherman, Howie Choset, and Daniel I Goldman. Frequency modulation of body waves to improve performance of sidewinding robots. *The International Journal of Robotics Research*, page 02783649211037715, 2021.
- [8] Baxi Chong, Yasemin O Aydin, Jennifer M Rieser, Guillaume Sartoretti, Tianyu Wang, Julian Whitman, Abdul Kaba, Enes Aydin, Ciera McFarland, Kelimar Diaz Cruz, et al. A general locomotion control framework for multi-legged locomotors. *Bioinspiration & Biomimetics*, 17(4): 046015, 2022.
- [9] Baxi Chong, Juntao He, Shengkai Li, Eva Erickson, Kelimar Diaz, Tianyu Wang, Daniel Soto, and Daniel I Goldman. Self-propulsion via slipping: frictional

- swimming in multi-legged locomotors. *arXiv preprint arXiv:2207.10604*, 2022.
- [10] Baxi Chong, Tianyu Wang, Eva Erickson, Philip J Bergmann, and Daniel I Goldman. Coordinating tiny limbs and long bodies: Geometric mechanics of lizard terrestrial swimming. *Proceedings of the National Academy of Sciences*, 119(27):e2118456119, 2022.
 - [11] Baxi Chong, Juntao He, Daniel Soto, Tianyu Wang, Daniel Irvine, and Daniel Goldman. A shannon-inspired framework for multi-legged matter transport. *Bulletin of the American Physical Society*, 2023.
 - [12] Abraham De Moivre. *Miscellanea analytica*. Tonson and Watts, London, 1730, 1730.
 - [13] Claire T Farley and C Richard Taylor. A mechanical trigger for the trot-gallop transition in horses. *Science*, 253(5017):306–308, 1991.
 - [14] Zipeng Fu, Ashish Kumar, Jitendra Malik, and Deepak Pathak. Minimizing energy consumption leads to the emergence of gaits in legged robots. *arXiv preprint arXiv:2111.01674*, 2021.
 - [15] Robert J Full and Daniel E Koditschek. Templates and anchors: neuromechanical hypotheses of legged locomotion on land. *Journal of experimental biology*, 202(23):3325–3332, 1999.
 - [16] Qinghong Guo, Mrinal K Mandal, and Micheal Y Li. Efficient hodge–helmholtz decomposition of motion fields. *Pattern Recognition Letters*, 26(4):493–501, 2005.
 - [17] Ross L Hatton and Howie Choset. Nonconservativity and noncommutativity in locomotion. *The European Physical Journal Special Topics*, 224(17-18):3141–3174, 2015.
 - [18] Milton Hildebrand. Symmetrical gaits of horses. *Science*, 150(3697):701–708, 1965.
 - [19] Milton Hildebrand. Symmetrical gaits of primates. *American Journal of Physical Anthropology*, 26(2):119–130, 1967.
 - [20] P Holmes, R J Full, D Koditschek, and J Guckenheimer. The Dynamics of Legged Locomotion: Models, Analyses, and Challenges. *SIAM Review*, 48(2):207–304, January 2006.
 - [21] Jemin Hwangbo, Joonho Lee, Alexey Dosovitskiy, Dario Bellicoso, Vassilios Tsounis, Vladlen Koltun, and Marco Hutter. Learning agile and dynamic motor skills for legged robots. *Science Robotics*, 4(26), 2019.
 - [22] Auke Jan Ijspeert, Alessandro Crespi, Dimitri Ryczko, and Jean-Marie Cabelguen. From swimming to walking with a salamander robot driven by a spinal cord model. *science*, 315(5817):1416–1420, 2007.
 - [23] Neri Kafkafi and Ilan Golani. A traveling wave of lateral movement coordinates both turning and forward walking in the ferret. *Biological Cybernetics*, 78(6):441–453, Jul 1998. ISSN 1432-0770. doi: 10.1007/s004220050448.
 - [24] Donghyun Kim, Jared Di Carlo, Benjamin Katz, Gerardo Bledt, and Sangbae Kim. Highly dynamic quadruped locomotion via whole-body impulse control and model predictive control. *arXiv preprint arXiv:1909.06586*, 2019.
 - [25] Joonho Lee, Jemin Hwangbo, Lorenz Wellhausen, Vladlen Koltun, and Marco Hutter. Learning quadrupedal locomotion over challenging terrain. *Science robotics*, 5(47):eabc5986, 2020.
 - [26] Chen Li, Tingnan Zhang, and Daniel I Goldman. A terradynamics of legged locomotion on granular media. *Science*, 339(6126):1408–1412, 2013.
 - [27] Junmin Li, Jinge Wang, Simon X Yang, Kedong Zhou, and Huijuan Tang. Gait planning and stability control of a quadruped robot. *Computational intelligence and neuroscience*, 2016, 2016.
 - [28] Bo Lin, Baxi Chong, Yasemin Ozkan-Aydin, Enes Aydin, Howie Choset, Daniel I Goldman, and Greg Blekherman. Optimizing coordinate choice for locomotion systems with toroidal shape spaces. In *2020 IEEE/RSJ International Conference on Intelligent Robots and Systems (IROS)*, pages 7501–7506, 2020. doi: 10.1109/IROS45743.2020.9341476.
 - [29] Andrew Lucas. Ising formulations of many np problems. *Frontiers in physics*, 2:5, 2014.
 - [30] Gabriel B Margolis and Pulkit Agrawal. Walk these ways: Tuning robot control for generalization with multiplicity of behavior. *arXiv preprint arXiv:2212.03238*, 2022.
 - [31] Jerrold E Marsden and Tudor S Ratiu. *Introduction to mechanics and symmetry: a basic exposition of classical mechanical systems*, volume 17. Springer Science & Business Media, 2013.
 - [32] Hamidreza Marvi, Chaohui Gong, Nick Gravish, Henry Astley, Matthew Travers, Ross L Hatton, Joseph R Mendelson, Howie Choset, David L Hu, and Daniel I Goldman. Sidewinding with minimal slip: Snake and robot ascent of sandy slopes. *Science*, 346(6206):224–229, 2014.
 - [33] LW McKeethan. A contribution to the theory of ferromagnetism. *Physical Review*, 26(2):274, 1925.
 - [34] Richard M Murray. *A mathematical introduction to robotic manipulation*. CRC press, 2017.
 - [35] Jong Hyeon Park and Ohung Kwon. Reflex control of biped robot locomotion on a slippery surface. In *Proceedings 2001 ICRA. IEEE International Conference on Robotics and Automation (Cat. No. 01CH37164)*, volume 4, pages 4134–4139. IEEE, 2001.
 - [36] Renfrey Burnard Potts. Some generalized order-disorder transformations. In *Mathematical proceedings of the cambridge philosophical society*, volume 48, pages 106–109. Cambridge University Press, 1952.
 - [37] Jennifer M Rieser, Chaohui Gong, Henry C Astley, Perrin E Schiebel, Ross L Hatton, Howie Choset, and Daniel I Goldman. Geometric phase and dimensionality reduction in locomoting living systems. *arXiv preprint arXiv:1906.11374*, 2019.
 - [38] Uluc Saranlı, Martin Buehler, and Daniel E Koditschek. Rhex: A simple and highly mobile hexapod robot. *The International Journal of Robotics Research*, 20(7):616–631, 2001.

- [39] Sangok Seok, Albert Wang, Meng Yee Chuah, Dong Jin Hyun, Jongwoo Lee, David M Otten, Jeffrey H Lang, and Sangbae Kim. Design principles for energy-efficient legged locomotion and implementation on the mit cheetah robot. *Ieee/asme transactions on mechatronics*, 20(3):1117–1129, 2014.
- [40] Sarah S Sharpe, Stephan A Koehler, Robyn M Kuckuk, Miguel Serrano, Patricio A Vela, Joseph Mendelson, and Daniel I Goldman. Locomotor benefits of being a slender and slick sand swimmer. *Journal of Experimental Biology*, 218(3):440–450, 2015.
- [41] Julian Whitman, Nico Zevallos, Matt Travers, and Howie Choset. Snake robot urban search after the 2017 mexico city earthquake. In *2018 IEEE international symposium on safety, security, and rescue robotics (SSRR)*, pages 1–6. IEEE, 2018.
- [42] Yuxiang Yang, Tingnan Zhang, Erwin Coumans, Jie Tan, and Byron Boots. Fast and efficient locomotion via learned gait transitions. In *Conference on Robot Learning*, pages 773–783. PMLR, 2022.
- [43] Tingnan Zhang and Daniel I Goldman. The effectiveness of resistive force theory in granular locomotion a. *Physics of Fluids*, 26(10):101308, 2014.